Simulating ship wave patterns through a 3D parallel SPH code

S. Marrone, B. Bouscasse, A. Colagrossi
CNR-INSEAN
Rome, Italy
s.marrone@insean.it, b.bouscasse@insean.it, a.colagrossi@insean.it

***Abstract*— An analysis of the 3D wave pattern generated by a ship in stationary forward motion is performed with a particular focus on the bow breaking wave. For this purpose a new 3D parallel SPH solver has been designed. An assessment of the capabilities of the 3D solver to perform wave breaking simulations is preliminarily performed on a test case specifically conceived. The numerical effort to simulate the complete evolution of the flow around the ship with sufficient resolution is considerable in 3D. Consequently, an ad hoc hybrid MPI-OpenMP parallelization has been developed to achieve simulations of hundred million of particles running on a computer cluster. The outcomes are compared with experimental measurements in terms of wave height and features of the bow wave.**

I. INTRODUCTION

The paper deals with the problem of a ship in steady-state forward motion with particular reference to the possibility of predicting the extent of breaking bow wave. From the physical point of view, it has been crucial for a long time to understand how bow waves are generated, and how they modify the flow field. The purpose was to improve the evaluation of the resistance. The progress given by the numerical and experimental study dedicated to the breaking phenomena have made possible to apprehend its effect on ship visibility.

At present, some numerical models for free-surface flows, in particular RANSE with level-set algorithm, are able to catch 3D breaking phenomena in bow waves (see for example Carrica et al. [1] and Di Mascio et al. [2]). SPH simulations have proven to be reliable over 2D breaking scenario. On the specific topic of bow waves, Colagrossi & al [3] proposed a 2D+t SPH model, and the computed flows qualitatively matched the breaking scenario. In Colagrossi [4], the prescriptions about the minimum discretization required to catch breaking inception were deeply investigated. In the present work, a 3D SPH solver is developed and tested in order to carry on the 3D wave pattern computation and the physical characterization of the bow wave.

The activity is complex, in fact simulations with varying spatial discretization require a *h-variable* formulation, see [5] and [6].

An assessment of the capabilities of the 3D solver to perform wave breaking simulations is performed on a test case specifically conceived. From the analysis of such test the minimum discretization necessary to describe the plunging jet is obtained and compared to previous 2D results from 2D+t analysis. The numerical effort to reach such a resolution in 3D for the ship bow wave is considerable because the fluid domain has to be large enough to simulate deep water behaviour and avoid wave reflections at the boundaries. The number of particles needed for these simulations is of the order of 10^8, therefore, an hybrid MPI-OpenMP parallelization has been developed. The SPH results obtained are then compared with experimental measurements and with simulations obtained by a RANSE solver coupled with a Level Set algorithm.

II. NUMERICAL SCHEME

A. SPH model adopted

The standard weakly-compressible SPH scheme is generally affected by some drawbacks. The main problems are the correct evaluation of the pressure values for strong impacts and the flickering of pressure profiles that may occur also in non-particularly violent flows. This is related to the fact that, in general, the SPH predicts kinematics very well but, conversely, large random pressure oscillations are present due to numerical high frequency acoustic signals.

Antuono et al. [7] added a numerical diffusive term in the density equation which smoothes out the numerical noise inside the pressure field. Further the model was proved to be consistent and convergent all over the fluid domain. Such a model is hereinafter referred as δ-SPH.

The discrete δ-SPH scheme proposed by Antuono et al. [7] reads:

$$\begin{cases} \dfrac{D\rho_i}{Dt} = -\rho_i \sum_j \left(\boldsymbol{u}_j - \boldsymbol{u}_i\right)\cdot\nabla_i W\left(\boldsymbol{r}_j\right)V_j + \delta h c_0 \sum_j \boldsymbol{\psi}_{ij}\cdot\nabla_i W\left(\boldsymbol{r}_j\right)V_j \\ \rho_i \dfrac{D\boldsymbol{u}_i}{Dt} = -\sum_j \left(p_j + p_i\right)\nabla_i W\left(\boldsymbol{r}_j\right)V_j + \rho_i \boldsymbol{f}_i + \alpha h c_0 \rho_0 \sum_j \pi_{ij}\nabla_i W\left(\boldsymbol{r}_j\right)V_j \\ p_i = c_0^2\left(\rho_i - \rho_0\right) \\ \dfrac{D\boldsymbol{r}_i}{Dt} = \boldsymbol{u}_i \end{cases}$$

where:

$$\boldsymbol{\psi}_{ij} = 2\left(\rho_j - \rho_i\right)\frac{\boldsymbol{r}_{ji}}{|\boldsymbol{r}_{ji}|^2} - \left[\langle\nabla\rho\rangle_i^L + \langle\nabla\rho\rangle_j^L\right], \quad \pi_{ij} = \frac{\left(\boldsymbol{u}_j - \boldsymbol{u}_i\right)\cdot\boldsymbol{r}_{ji}}{|\boldsymbol{r}_{ji}|^2},$$

and $r_{ji} = r_j - r_i$. The symbol $\langle\nabla\rho\rangle_i^L$ indicates the renormalized gradient defined in [23343]. The symbols ρ_i, p_i and u_i denote the i-th particle density, pressure and velocity. Coefficients δ and α control the order of magnitude of the diffusive term and of the artificial viscous term respectively. Typical values are $\alpha = 0.01$, $\delta = 0.1$. The system (3.1.5) preserves the global mass and both the linear and angular momenta. Finally, the diffusive term inside the continuity equation and the artificial viscosity term go to zero as far as the spatial resolution increases. In this way the consistency with the Euler equations is recovered.

For what concern the boundary treatment the problem of flow around a ship in constant forward motion requires the definition of suitable inflow/outflow boundary condition to model the flow current. This is achieved through an extension to 3D of the algorithm proposed by Federico et al. [8] where buffer zones are defined to reproduce in/out-flow conditions. Moreover, in order to enforce solid boundary conditions along the ship hull and side and bottom walls, a robust and simple method is needed. To this purpose, the technique presented by De Leffe et al. [9] has been adopted.

B. *Parallelization strategy*

In order to perform an expensive computation like the bow wave breaking, it is necessary to develop an *ad-hoc* 3D parallel solver able to run efficiently on a cluster. The solver has been developed targeting a simulation of hundreds of millions of particles.

Because of the Lagrangian nature of the SPH model the parallelization of the code is non trivial and specific algorithms for this aim have to be designed and validated. Indeed, as opposed to mesh-based methods for which a fixed grid is employed, the SPH method relies on moving particles advected by the calculated fluid flow. Depending on the problem to solve, large particle displacements may occur. The parallel scheme should necessarily take this specificity into account. This Lagrangian characteristic also implies a major disorder of the particles, and therefore of scattered data in memory. Note that for mesh-based methods, the connections are fixed during the calculation: the neighbourhood of a given cell of interest remains the same throughout the calculation. Thus, a recurrent pattern of interpolation can be used, simplifying the parallelization scheme. Unfortunately, such a simplification is not possible in the SPH formalism. Indeed, the neighbourhoods of SPH particles are constantly changing during the calculation, requiring a special procedure for updating neighbourhoods. The parallelization is thereby affected. More precisely the core of the parallel algorithmic structure naturally revolves around a neighbour search procedure. Therefore, the issues for which most care has to be paid are the communication of neighbouring particles belonging to different processors and the update and trade-off of processors working load.

The parallelization strategy here adopted takes advantage of a MPI domain decomposition, realized in a very simple but effective manner, coupled with a OpenMP data decomposition in order to take advantage of the shared memory architectures.

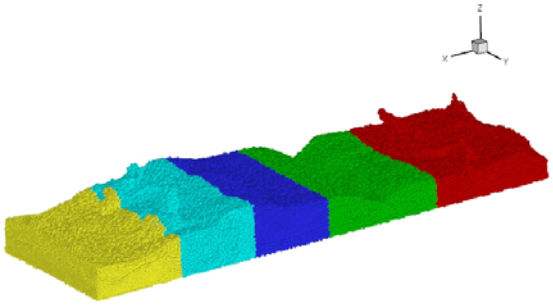

Figure 1. Example of division of the fluid domain over processors.

In order to simplify the MPI parallelization procedure and make the code faster some specific hypothesis have been assumed in the present problem.

In simulating ship wave the fluid domain is characterized by a dominant length corresponding to the main flow direction. Therefore it is possible to divide the fluid domain into parallel slices along the main flow direction, say the *x-axis*, equally balancing the number of particles per processor (Figure 1). In this way there is just one direction of communication between adjacent nodes. It allows simplifying the parallelization algorithm: the more the simulated phenomenon has a principal direction of evolution, the more the parallelization will be efficient.

Generally in common SPH practice it is useful and fast for the neighbour search to create a regular grid overlapping the computational domain. Each cell of the grid is a cube with size equal to the kernel radius. In this way the neighbours of each particle are found in the cells surrounding the particle's one (Linked-List algorithm). At each time step the list of particles and their belonging cells are calculated. In order to further simplify the problem, the computational domain is separated into domains that rely on the grid used for particle neighbour search.

The idea is to use this grid to speed up the operations between processors. Since the list of the particles belonging to different cells is already calculated, it can be used to quickly update the list of particles belonging to different processors and to determine the buffer particles to be communicated to the adjacent processors. Considering a single processor, the buffer particles are virtual particles that are received from the two adjacent processors and are needed to complete the interpolation of particles placed in proximity of the processor boundaries. In other words the buffer particles give contributions to the equation of motion of the local particles but their physical quantities are not updated because they belongs to another processor .

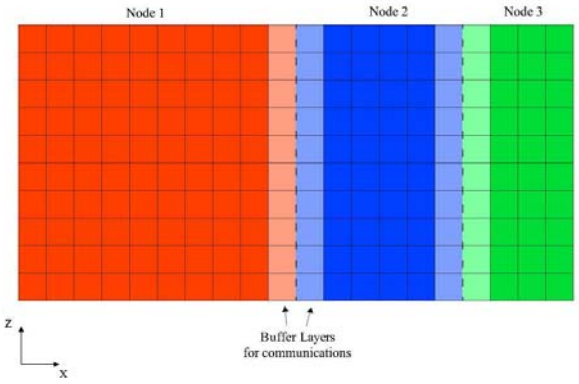

Figure 2. Sketch of the cell grid and processor sub-domains

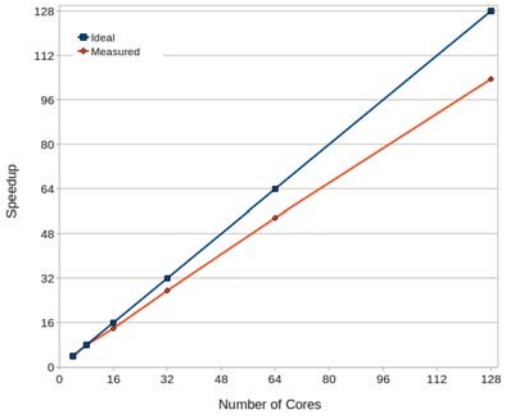

Figure 3. Overall speed-up obtained for simulating a flow around a ship. Up to16 cores only MPI parallelization is used, Points 32, 64, and 128 cores are obtained with the combination of 16 MPI nodes with respectively 2, 4 and 8 OpenMP threads

According to the parallelization strategy adopted, each processor extends over a finite number of cells along the *x-axis*, overlapping for one cell the adjacent processors (see Figure 2.), while it covers all the computational domain along the *y-axis* and *z-axis*. In this way, a single layer of cell is scanned looking for particles to be sent to adjacent processor as buffer particles. At each time step, the buffer particles of the buffer layers are sent and received by processors through synchronous send/receive MPI communications. Synchronous communication are not the most efficient but are safer in term of robustness and code simplicity. Anyway, there are at most two communication stages (just two adjacent processors) per time step and, consequently, time consumption due to communications is negligible respect to computations. With this approach, it is also straightforward for each processor to update its belonging particles. As already mentioned, the Lagrangian particles cross naturally the processors boundaries. These particles are sent together with buffer particles and hence are assigned in the cells of the receiving processor. Then, each processor scans the cells of its own sub-domain to update the list of particles.

For the problem of the flow around a ship in forward motion an example of the overall speedup is displayed in Figure 3. . In particular the simulation considered is the flow around the ship that involves 8 millions particles. The result presented clearly shows the effectiveness of the parallelization strategy adopted. Indeed, simulations can be run up to 128 cores with a fair scalability.

III. PRELIMINARY COMPUTATIONS USING A SIMPLIFIED GEOMETRY

In order to test the capacity of the 3D SPH code to simulate the breaking wave, a special test is devised. The geometry is a channel where the right wall (when looking toward the outflow) is a ruled surface. The flow encountering it creates an overturning wave generating intense splash-up cycles. A forced inflow is fixed and a free outflow condition is given. For what concern the lateral and bottom boundaries, solid walls are used. The geometry looks similar to a ship bow characterized by a large flare, see Figure 4. Figure 5. . The height of the water inflow is $H=1\ m$. The non dimensional velocity of the flow is $Fn_H = U_{Flow}/\sqrt{gH} = 2$. The ruled surface, say S, can be derived as a linear combination of the parametric representation of two lines $\alpha(t)$ and $\beta(t)$ as follows:

$$S(t,u) = u\alpha(t) + (1-u)\beta(t), \quad u \in [0,1], t \in [0,5]$$

$$\alpha : \begin{cases} x = 5 \\ y = 0 \\ z = t \end{cases}, \qquad \beta : \begin{cases} x = 5 + L \\ y = \dfrac{\sqrt{2}}{2}t + \dfrac{L}{4} \\ z = \dfrac{\sqrt{2}}{2}t \end{cases}$$

The overturning jet generated has a height of $H_{pj} \cong 0.5H$. Two tests with different spatial resolution are performed in order to verify the capability of the solver to simulate the breaking waves (see Table I). In Figure 6. , transversal cuts related to test *Break1* and *Break2* are shown just before the closure of the plunging jet. It has to be noticed that the longitudinal position corresponding to the closure is not exactly the same in the two cases. The spatial resolution of test *Break1* is insufficient to reproduce the plunging jet.

TABLE I. PRELIMINARY COMPUTATIONS

	Hpj	**Npart(.10^6)**	**H_{pj}/dx**	**dx**
Break1	0,5	4	12,5	0,04
Break2	0,5	32	25	0,02

In Figure 7. Figure 8. Figure 9. , the free-surface evolution is shown at $t=18(H/g)^{1/2}$, for test *Break2*, when the wave front reaches a steady state. In particular, in Figure 7. , clear scar-lines are visible on the free surface. Those are generated by vortical structures induced by the splash-up process. Figure 8. shows a 3D view where the free-surface is coloured according to the modulus of the vorticity.

Figure 9. shows the entrapment of the two layers of particles closest to free surface at the inflow.

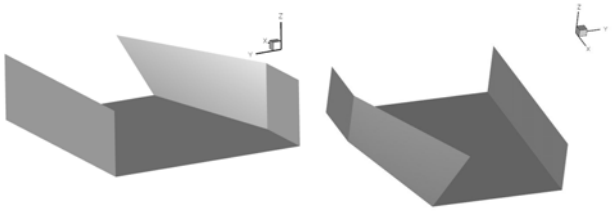

Figure 4. Geometry of the channel used to generate an overturning wave. View from the inflow (left) and the outflow (right).

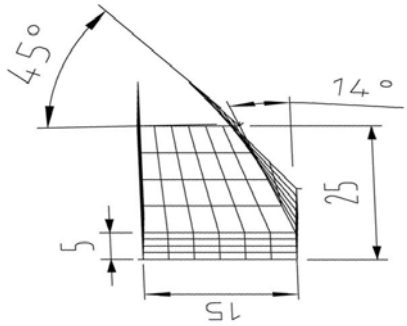

Figure 5. Sketch of the channel.

The SPH lagrangian tracking clearly highlights the generation of four longitudinal (x-axis) vortical tubes shed by the breaking wave front. A fifth smaller vortical structure occurs just below the front in the form of a quasi-steady spilling breaker. All these flow features can be observed just in the *Break2* test case where the spatial discretization is sufficient to discretize the plunging jet with a suitable number of particles.

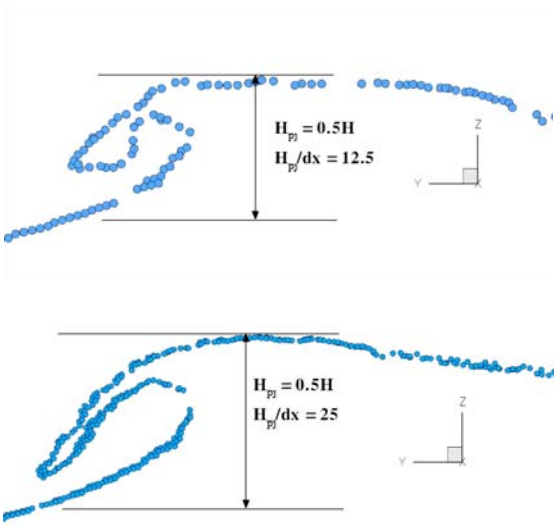

Figure 6. Transversal cut for the case *Break1* (top) and *Break2 (bottom)*

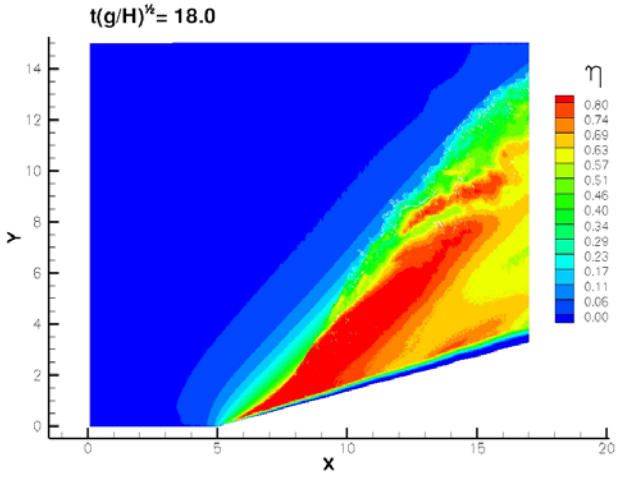

Figure 7. Wave elevation at the steady state.

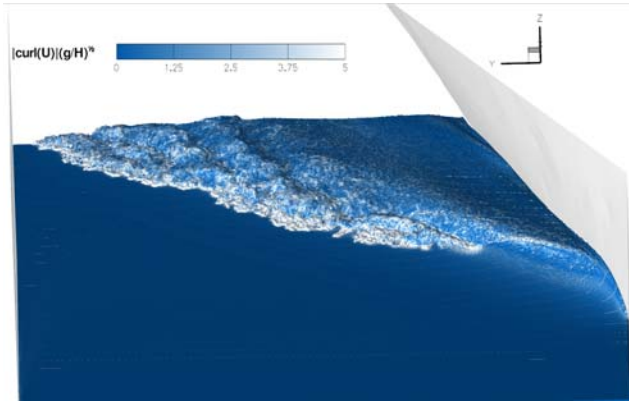

Figure 8. Contour of the modulus of the vorticity, $t=18(H/g)^{1/2}$

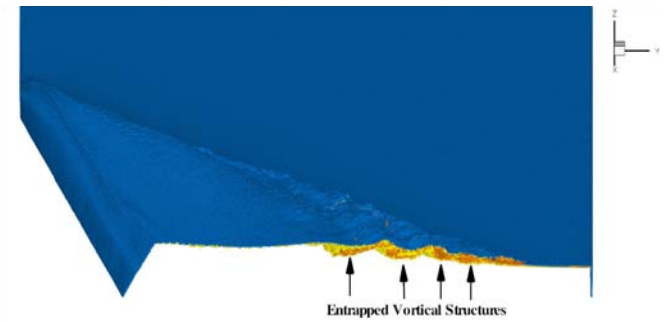

Figure 9. 3D view of the of the overturning wave generated in a be, steady-state condition, $t=18(H/g)^{1/2}$

IV. DESCRIPTION OF THE PROBLEM

A. *Description of the computational domain*

The main objective of the this work is to simulate the free surface flow around the hull of the Alliance ship in forward motion, see Figure 11. and Table II for characteristics and body plan. The study is divided in two parts:

- the validation of the code on the global wave pattern;
- a detailed study on the evolution of the bow wave and the breaking inception.

The simulations are solved in the frame of reference of the ship, z is the vertical axis (opposite sense respect to gravity), x the longitudinal axis of the hull (positive towards outflow), and y the transversal axis of the model. A forced inflow is fixed at a certain distance from the bow, and a free outflow condition is given the farther possible from the stern. For what concern the lateral and bottom boundaries, solid walls are used (no models to enforce the radiation condition are present in SPH literature). A sketch of the numerical domain is depicted in Figure 10. .

The numerical effort to reach a sufficient discretization is considerable in 3D because the fluid domain has to be sufficiently large to simulate a deep water behaviour and avoid wave reflections at the boundaries. The resulting testing condition is therefore necessarily a compromise.

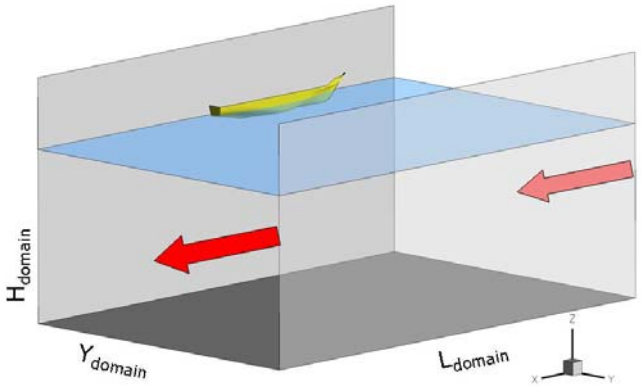

Figure 10. Sketch of the problem

B. *Pre-processing of ship geometry*

The body surface is defined in the solver by a list of points and associated normal vectors. Each point represents a piece of surface. The discretization of the body surface is achieved importing the CAD design into a software for mesh generation. A triangularization of the surface is performed and the area and normal of each triangle is associated with each point placed at the centroid. The numerical scale of the ship model is displayed in Table II while the ship body plan of the Alliance vessel is depicted in Figure 11. .

TABLE II. ALLIANCE SHIP PARAMETERS

	Full Scale	Numerical Scale
Length Lpp (m)	82	1
g (m.s^{-2})	9.81	1
Breadth B (m)	15.2	0.186
Draft D (m)	5.2	0.063
Displacement Δ	2920 t	5.3 m^3

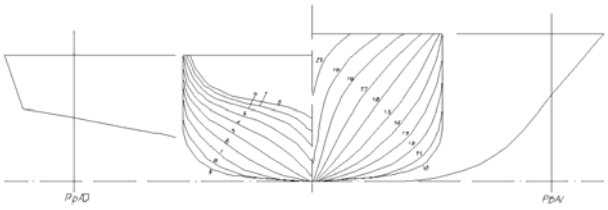

Figure 11. Body plan of the Alliance vessel.

C. *Remarks on breaking bow wave from the 2D+t analysis*

For high or medium Froude numbers, the evolution of the bow breaking wave is characterized by the generation of a first plunging jet that triggers a cyclic splash-up process. In the evolution of this phenomenon several vortical structures are shed in the wake inducing scar-lines on the free surface. More details are given in [4] where the relation between the intensity of the breaking, the size of the plunging-jet and the forward velocity was investigated.

The Froude number of the computation is set to *Fn=0.328* (18.1 knots in full scale) in order to compare the numerical outcome with the experimental data [11].

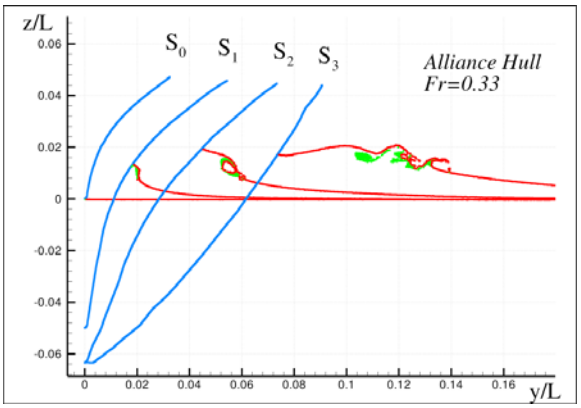

Figure 12. *2D+t:* snapshots of the evolution for *Fr = 0.33.* Sections S_0 (x/L = 0.0160), S_1 (x/L = 0.0685), S_2 (x/L = 0.1360), S_3 (x/L = 0.2485).

2D+t calculation has been performed for *Fn=0.334*, the main results are shown in Figure 12. . The plunging jet has a characteristic height of $H_{pj} = 0.01L$ therefore it is very small and very challenging to be captured in 3D simulations. As shown in [10] a proper spatial discretization is needed to discretize the plunging jet. The *2D+t* analysis also suggests that the relation

$$H_{pj} / h > 20 \quad (1)$$

has to be verified where h the SPH smoothing length. This relation in our case is equivalent to $D = 120h$, where D is the ship draft.

Note that the result given by the *2D+t* simulations - relation *(1)* – is almost the same obtained in section III where 3D breaking wave is simulated around a simplified ship-like geometry.

V. DISCUSSION OF THE RESULTS

In this section, the INSEAN SPH code is validated on the global wave pattern and on the breaking bow wave pattern generated by the Alliance vessel. The numerical simulations are compared with the experimental data from DGA-Hydrodynamics, see [11]. The origin is fixed at the intersection between the still water level and the first perpendicular of the ship. The *x* axis points as the forward velocity.

TABLE III. WAVE AND BOW PATTERN COMPUTATIONS

	X_{min}	X_{max}	Y_{max}	Z_{min}	$N_{part}(E^6)$	D/dx	t_f $(g/L)^{1/2}$	dx/L	Mul-res ratio
Test4	-0,26	1	0,8	-0,26	17	25,2	5	0,0025	1
Test5	-0,26	2	0,8	-0,56	65	25,2	10	0,0025	1
Test6	-0,26	1	0,8	-0,26	22	38	4	0,0017	1.5
Test7	-0,26	1	0,8	-0,26	145	75,9	4	0,0008	1.5

In Table III details of the SPH computations are given. *Test4* and *Test5* are performed with the same resolution but for two different sizes of the domain. *Test6* and *Test7* are obtained using the domain but with a multi-resolution technique explained in paragraph *B*.

A. *Analysis of the global wave pattern*

We start the analysis of the global wave pattern using the SPH results for the *Test5* of Table III.

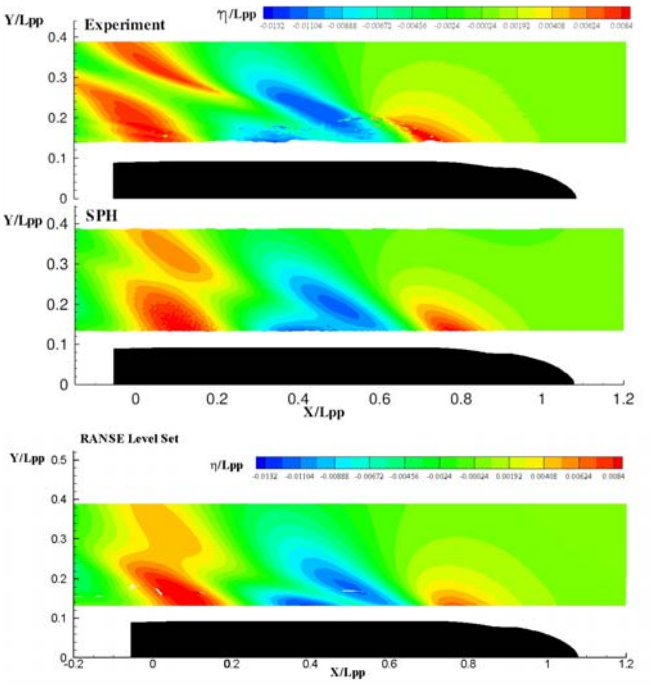

Figure 13. Contours of the wave elevation for Fn 0.328: top panel experimental results from DGA-HYDRODYNAMICS; middle panel SPH results; bottom panel RANSE results.

Top plot of Figure 13. reports experimental measurements of the wave elevation. The middle plot of Figure 13. shows the SPH wave contour while bottom panel shows the same field obtained by a RANSE code (INSEAN *Xnavis* code [2]) at the same condition. The global agreement is fair, the SPH result appears to be close to the RANSE calculation and agrees slightly better with the experiments. The rear divergent waves appear underestimated by both the numerical simulations. From the experiment it seems that the breaking bow wave affects the wave pattern close to the bow region as well as the rear divergent wave. In particular in Figure 14. a dashed line is drawn to highlight the region of influence of the breaking bow wave on the rear wave pattern. This region is characterized by high curvature of the free-surface which are not resolved in both simulations. Indeed, the discretization adopted is not sufficient to capture the breaking wave phenomena and its influence on the wave pattern.

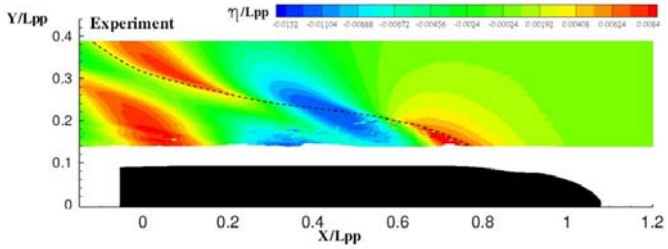

Figure 14. Contours of the experimental wave elevation for Fn 0.328 (results from DGA-Hydrodynamics). The dashed line highlights the effect of the breaking bow wave on the rear wave pattern.

B. *Focus on the bow wave*

To capture the physics of the breaking wave, the resolution has to be increased. On the other hand increasing resolution maintaining the computational domain of *Test5* is not practically possible with the available resources. Then, a run with smaller domain is attempted in *Test4 (*see Table III). The field is reduced in 2 directions, the water height (Z_{min}) and the outflow position (X_{max}). Even if the higher bottom induces non-negligible effects, it is observed that the main characteristics of the wave pattern are preserved until $t(g/L)^{1/2} = 4$ since the wave field is deformed by the outflow as shown in Figure 15. . Anyway the bow region is kept almost undisturbed. Comparing the results of *Test4* with the one obtained in *Test5*, one can observe the wave fields are similar up to $x=0.5L$. Therefore, the main idea is to capture the breaking bow wave performing a simulation with a domain extension equal to *Test4* in a time interval equal to $t(g/L)^{1/2} = [0, 4]$ with a spatial resolution three times higher.

To further increase the spatial discretization, a multi resolution technique has been adopted in a similar way as in [4]. On a band of thickness *0.25D* close to the free surface, the ratio *h/dx* is set equal to *1.33* (266 neighbours). The band's thickness is given by the maximum depth reached by vortical structures discussed in [4]. The ratio *h/dx* is reduced

to *0.90* (80 neighbours) for the rest of the domain where small gradients of flow field occurs. In this way the size of particles in the low-resolution zone are larger by a factor *1.5* (*multi-resolution ratio* in Table III). A new test *Test6* is done in order to verify the robustness and the correctness of the solution with this technique. The size of the domain are the same as in *Test4,* and the discretization of the low-resolution region is the same. Figure 16. shows the wave pattern given by *Test6* maching the pattern from *Test4*, demonstrating the validity of the proposed multi-resolution technique.

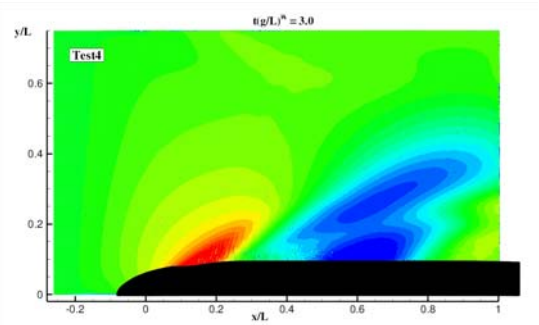

Figure 15. Wave pattern case *Test4*

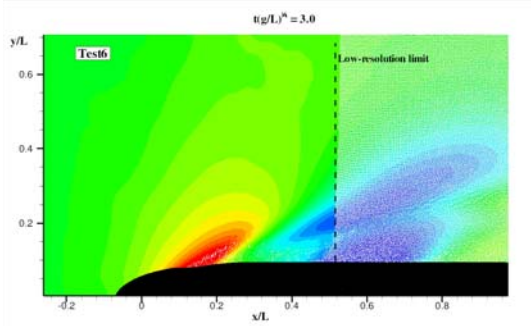

Figure 16. Wave pattern case *Test6*

Test7 is designed with a spatial resolution large enough to capture the breaking of the bow wave. From Figure 17. it is possible to observe that the shape of the bow wave obtained in *Test7* is closer to the experimental one respect to *Test5*. Unfortunately the limited extensions of domain in *Test7* does not permit to highlight the effect of the bow wave breaking on the rear part of the wave pattern. In Figure 19. a 3D view of the bow wave simulated in *Test7* is shown. From a qualitative comparison with the picture of Figure 18. taken at DGA-Hydrodynamics it is possible to observe that the global behaviour of the phenomenon is retained. In Figure 20. the top view of the bow wave is depicted. From a comparison with Figure 15 it is possible to notice that the extension and the shape of the breaking zone is well reproduced.

Anyway, the resolution is still slightly insufficient to fully resolve all the breaking features. Indeed, the SPH seems to reproduce only a typical spilling breaking evolution while in Figure 21. it is evident that energetic splash-up occur. This is in accordance with *2D+T* simulations carried out in [10] where two splash-up cycles are present in the simulation with Fn 0.33.

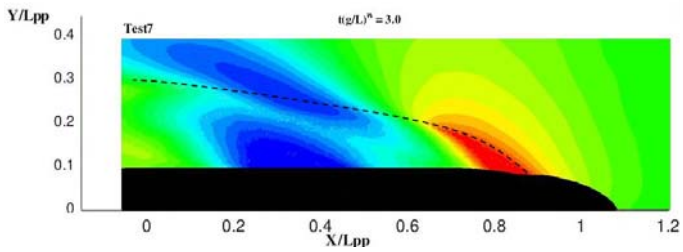

Figure 17. Contours of wave elevation for SPH simulation Test7. The dashed line highlights the breaking wave front.

Figure 18. Breaking bow wave during experiments at DGA-Hydrodynamics, Fn 0.328

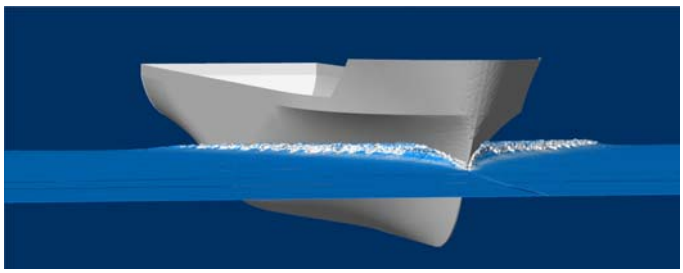

Figure 19. 3D view of the breaking bow wave in the SPH simulation Fn = 0.328

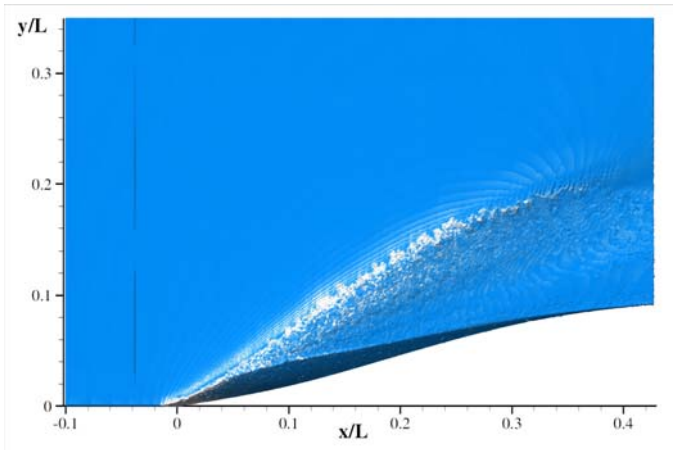

Figure 20. Top view of the breaking bow waves in the SPH simulation Fn = 0.328

Figure 21. Details of the breaking bow wave during experiments at DGA-Hydrodynamics, Fn 0.328

VI. CONCLUSIONS

A 3D SPH solver has been applied to simulate the wave pattern generated by a slender ship in stationary forward motion. New parallel algorithms have been developed and tested. A particular attention has been given to the bow breaking wave phenomenon. The outcomes have been compared with experimental results and a RANSE level set computation. The activity is ambitious, in fact the SPH method has not a good capacity to perform simulations where spatial discretization is characterized by high spatial gradients, as requested by the problem. A feasibility analysis based on results of a *2D+T* study is conducted to set-up a suitable simulation taking into account the computational possibilities. Preliminary simulations are performed to evaluate the minimal resolution needed to catch the bow breaking wave and in order to identify the smaller numerical domain guaranteeing the correctness of the solution.

Further, a detailed validation is conducted on the global wave pattern. The results show a fair agreement with both results of RANSE calculations and experimental measurements. For what concerns the study of the breaking bow wave future works will be devoted on the development of techniques focused to manage multi-resolution techniques needed to properly catch such a phenomena.

ACKNOWLEDGEMENT

This work has been done in the framework of Research Project EUROPA ERG1 RTP N°110.067 “Development and Validation of Tools for the Prediction of Hydrodynamics Signatures”, DALIDA, financially supported by the Italian and the French Navies, throughout the European Defence Agency, for which activities include experimental tests in both calm water and in waves, as well as complementary numerical simulations. Numerical computations presented here have been performed on the parallel machines of CASPUR Supercomputing Center (Rome); their support is gratefully acknowledged. This work was also partially supported by European Community's Seventh Framework Programme (FP7/2007-2013) under grant agreement n225967 “NextMuSE”.

REFERENCES

[1] P. M. Carrica, R. V. Wilson, and F. Stern, “ Free surface flows around ships: progress toward simulation of high-speed flows and motions” in Mécanica Computacional, vol. XXIV Eds. A. Larreteguy: 2005.

[2] A, Di Mascio, R. Broglia and R. Muscari, “On the application of the single-phase level set method to naval hydrodynamic flows” in computers & fluids, vol. 36, Eds. Elsevier: 2007, pp. 868–886.

[3] A. Colagrossi, M. Landrini, and M. P. Tulin, “Numerical studies of wave breaking compared to experimental observations”. 4th Numerical Towing Tank Symposium (NuTTS), Hamburg : 2001.

[4] A. Colagrossi, , M. Antuono, and S. Marrone, “A 2D+t SPH model with enhanced solid boundary treatment”. 4th international SPHERIC, Nantes: 2009.

[5] L. Hernquist and N. Katz, “TREESPH: a unification of SPH with the hierarchical tree method, The Astrophysical J. Supp. Ser, 70, pp 419-446: 1989

[6] R.P. Nelson and J.C.B. Papaloizou, “Variable smoothing lengths and energy conservation in SPH”, Mon. Not. R. Astronom. Soc., 270, pp 1-20: 1994

[7] M. Antuono,A. Colagrossi, S. Marrone, D. Molteni, “Free-surface flows solved by means of SPH schemes with numerical diffusive terms”, Computer Physics Communications, **181**(3): 532-549: 2009

[8] I. Federico, S. Marrone, A. Colagrossi, F. Aristodemo, P. Veltri. Simulating free-surface channel flows through SPH, Proc. V International SPHERIC Workshop, Manchester 2010.

[9] M. De Leffe, D. Le Touzé, B. Alessandrini. “Normal flux method at the boundary for SPH”, Proc. IV International SPHERIC Workshop, Nantes 2009.

[10] S Marrone, M Antuono and Andrea Colagrossi, “INSEAN Technical Report, Task N5.IN2”, INSEAN, Technical report DALIDA project.

[11] O.Perelman, “Minutes of towing tank test, Task E6.BE2”, DGA-Hydrodynamics, Technical report Dalida project.